



A Radio Frequency Study of the Accreting Millisecond X-ray Pulsar, IGR J16597–3704, in the Globular Cluster NGC 6256

A. J. Tetarenko¹ , A. Bahramian² , R. Wijnands³, C. O. Heinke¹ , T. J. Maccarone⁴, J. C. A. Miller-Jones⁵ , J. Strader² , L. Chomiuk² , N. Degenaar³, G. R. Sivakoff¹ , D. Altamirano⁶ , A. T. Deller⁷ , J. A. Kennea⁸ , K. L. Li² , R. M. Plotkin⁵ , T. D. Russell³ , and A. W. Shaw¹

¹ Department of Physics, University of Alberta, CCIS 4-181, Edmonton, AB T6G 2E1, Canada; tetarenk@ualberta.ca

² Department of Physics and Astronomy, Michigan State University, East Lansing, MI, USA

³ Anton Pannekoek Institute for Astronomy, University of Amsterdam, Science Park 904, 1098 XH Amsterdam, The Netherlands

⁴ Department of Physics and Astronomy, Texas Tech University, Box 41051, Lubbock, TX 79409-1051, USA

⁵ International Centre for Radio Astronomy Research, Curtin University, G.P.O. Box U1987, Perth, WA, 6845, Australia

⁶ Physics and Astronomy, University of Southampton, Southampton SO17 1BJ, UK

⁷ Centre for Astrophysics and Supercomputing, Swinburne University of Technology, Hawthorn, VIC 3122, Australia

⁸ Department of Astronomy and Astrophysics, Pennsylvania State University, 525 Davey Lab, University Park, PA 16802, USA

Received 2017 November 30; revised 2018 January 9; accepted 2018 January 17; published 2018 February 20

Abstract

We present Karl G. Jansky Very Large Array radio frequency observations of the new accreting millisecond X-ray pulsar (AMXP), IGR J16597–3704, located in the globular cluster NGC 6256. With these data, we detect a radio counterpart to IGR J16597–3704, and determine an improved source position. Pairing our radio observations with quasi-simultaneous *Swift*/*XRT* X-ray observations, we place IGR J16597–3704 on the radio–X-ray luminosity plane, where we find that IGR J16597–3704 is one of the more radio-quiet neutron star low-mass X-ray binaries known to date. We discuss the mechanisms that may govern radio luminosity (and in turn jet production and evolution) in AMXPs. Furthermore, we use our derived radio position to search for a counterpart in archival *Hubble Space Telescope* and *Chandra X-ray Observatory* data, and estimate an upper limit on the X-ray luminosity of IGR J16597–3704 during quiescence.

Key words: globular clusters: individual (NGC 6256) – ISM: jets and outflows – radio continuum: stars – stars: individual (IGR J16597–3704) – stars: neutron – X-rays: binaries

1. Introduction

Relativistic jets are launched from many different types of accreting stellar-mass compact objects (black holes, neutron stars, and possibly white dwarfs; Fender 2006; Migliari & Fender 2006; Körding, et al. 2008; Coppejans et al. 2015; Russell et al. 2016); however, our current knowledge of the physics that gives rise to and governs jet behavior is still somewhat limited. A crucial step toward understanding the mechanisms that drive jet behavior is characterizing jet properties (and how these properties are coupled to the conditions in the accretion flow) in different accreting systems across the mass scale.

A key observational diagnostic for comparing jet properties between different systems is the radio–X-ray correlation, relating radio and X-ray luminosities ($L_R \propto L_X^\beta$, where β represents the disk-jet coupling index; Gallo et al. 2003; Corbel et al. 2013). This empirical relationship, which couples a compact, partially self-absorbed synchrotron jet (probed by radio emission) to the properties of the accretion flow (probed by X-ray emission), has been well studied in black hole X-ray binary systems (BHXBs; binary systems harboring a black hole accreting matter from a companion star). In particular, different BHXB systems, sampled over several orders of magnitude in X-ray luminosity, are known to display correlations that range from $\beta \sim 0.6$ –1.8 (potentially following one of two tracks in the radio–X-ray plane at $L_X > 10^{36}$ erg s^{−1}; Coriat et al. 2011a; Gallo et al. 2014; Russell et al. 2015). However, the different classes of neutron star X-ray binary systems (NSXBs; binary systems harboring a neutron star accreting matter from a companion star) are not as well sampled (in particular due to

the limited range of X-ray luminosities that have been sampled to date), and have shown more complex behavior in the radio–X-ray plane, as compared to the BHXBs.

While NSXBs are generally more radio-quiet than BHXBs, different neutron star X-ray binary classes have shown varying correlation indices⁹ and normalizations in the radio–X-ray plane (Migliari et al. 2003; Migliari & Fender 2006; Tudose et al. 2009; Miller-Jones et al. 2010b; Tetarenko et al. 2016; Tudor et al. 2017). For example, some non-pulsating neutron stars display $\beta \sim 1.4$ (Migliari & Fender 2006; Miller-Jones et al. 2010b), while some accreting millisecond X-ray pulsars (AMXPs; accreting neutron star binaries where X-ray pulsations at the spin period of the neutron star are observed) and three transitional millisecond X-ray pulsars (tMSPs; accreting neutron star binaries that switch between a rotation-powered pulsar state and an accretion-powered state; Archibald et al. 2009; Papitto et al. 2013; Bassa et al. 2014; Patruno et al. 2014) have been suggested to follow a shallower correlation of $\beta \sim 0.7$ (Deller et al. 2015). Furthermore, differences are also observed between individual systems of the same class. For example, recent work has shown that not all AMXPs and non-pulsating NSXBs follow the above mentioned “standard” tracks in the radio–X-ray plane (where some systems may display lower/higher radio luminosities; Tetarenko et al. 2016; Tudor et al. 2017). Many different factors could play a role in causing these observed differences,

⁹ We note that these correlation indices are measured over a limited range of X-ray luminosity, and Corbel et al. (2013) found that an X-ray luminosity lever arm extending across at least 2 dex is needed to accurately measure a correlation in the radio–X-ray plane.

Table 1
Radio and X-Ray Observation Details and Luminosities for IGR J16597–3704

Epoch	Radio Observation (dd/mm/yy, UTC)	X-ray Observation (dd/mm/yy, UTC)	$L_{5\text{ GHz}}^{\text{a,b}}$ ($\times 10^{28}\text{ erg s}^{-1}$)	$L_{1-10\text{ keV}}^{\text{a}}$ ($\times 10^{36}\text{ erg s}^{-1}$)
1	23 Oct 2017, 21:01–22:42	22 Oct 2017, 20:29–20:47	0.87 ± 0.22	2.69 ± 0.11
2	27 Oct 2017, 20:44–22:25	25 Oct 2017, 07:30–07:51	1.20 ± 0.21	2.76 ± 0.08

Notes.

^a To calculate the luminosities, we use a distance to NGC 6256 of $D = 9.1\text{ kpc}$ (Valenti et al. 2007). Uncertainties include measurement errors only, and are quoted at the 1σ level.

^b We calculate 5 GHz radio luminosities ($L_R = \nu L_\nu$) by combining the two VLA basebands in each observation and assuming a flat spectral index to extrapolate to 5 GHz.

such as variations in jet power, compact object mass, spin, magnetic field, and jet launching mechanism. To disentangle these factors, as well as understand the reason(s) for a lack of clear correlation(s) and the wide range of radio luminosities observed in neutron star systems, constraints from a larger population of neutron star systems (especially at $L_X < 10^{36}\text{ erg s}^{-1}$), are strongly needed. However, sampling neutron star systems at X-ray luminosities between $10^{34} < L_X < 10^{36}\text{ erg s}^{-1}$ is observationally challenging, as neutron stars tend to evolve quickly in this luminosity range and are faint at radio frequencies. Rapid, coordinated radio and X-ray observations of new X-ray transients discovered in our Galaxy can in principle provide these much needed constraints.

IGR J16597–3704 is a new X-ray transient discovered with the *INTErnational Gamma-Ray Astrophysics Laboratory* (*INTEGRAL*) on 2017 October 21 (Bozzo et al. 2017a). Follow-up *Swift* X-ray Telescope (XRT; Burrows et al. 2005) observations (Bozzo et al. 2017b) on 2017 October 22 confirmed the presence of a new bright X-ray source within the *INTEGRAL* error circle, and placed this new transient in the globular cluster NGC 6256 ($D = 9.1\text{ kpc}$; Valenti et al. 2007). To determine the nature of IGR J16597–3704 and localize its position, we performed NSF’s Karl G. Jansky Very Large Array (VLA) radio frequency observations of IGR J16597–3704 on 2017 October 23 and 27 (Tetarenko et al. 2017a). These radio observations were taken within 3 days of *Swift*/*XRT* observations of the source, allowing us to also place this new source in the radio–X-ray correlation plane. The preliminary position of IGR J16597–3704 on the radio–X-ray plane strongly suggested that this new transient is a neutron star system. This classification was confirmed by Sanna et al. (2017), who reported the discovery of X-ray pulsations, finding that IGR J16597–3704 is an ultra-compact binary (~ 46 minute orbital period), with a short spin period (9.5 ms), and suggested a high magnetic field ($9.2 \times 10^8 < B < 5.2 \times 10^{10}\text{ G}$). IGR J16597–3704 was also observed with *Chandra* on 2017 October 25 (Chakrabarty et al. 2017). In this paper, we report on our VLA radio and *Swift*/*XRT* X-ray observations, as well as our search for the optical and quiescent X-ray counterparts to IGR J16597–3704.

2. Observations and Data Analysis

2.1. VLA Radio Observations of IGR J16597–3704

IGR J16597–3704 was observed with the VLA (project code VLA/17B-257) over two epochs, 2017 October 23 and 27 (see Table 1 for observation times), with 88.6 min on source at each epoch. The array was in its B configuration, with a beam size of $2.2 \times 0.8\text{ arcsec}$. All observations were taken

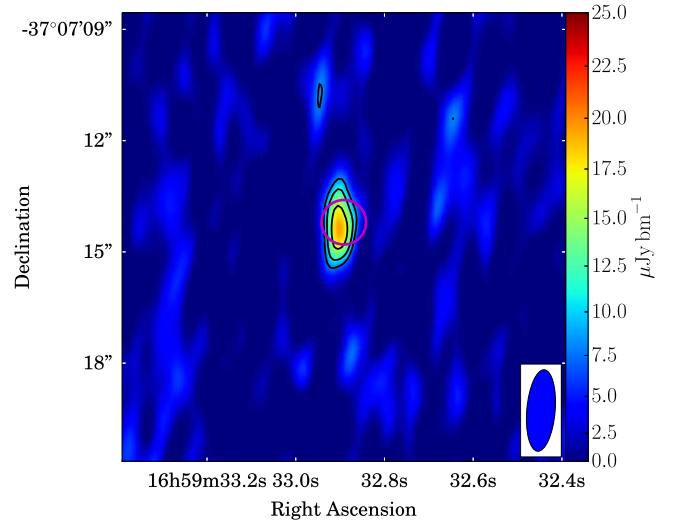


Figure 1. VLA radio image of IGR J16597–3704 taken at 10 GHz. We produced this image by stacking the data of both VLA epochs in the uv -plane. The source is clearly detected in the image, where contour levels are $2^{n/2} \times$ the rms noise of $2.8\ \mu\text{Jy bm}^{-1}$, with $n = 3, 4, 5$. The color bar represents the flux density in units of $\mu\text{Jy bm}^{-1}$, and the blue ellipse is the VLA beam (the elongated beam shape is due to the low declination of IGR J16597–3704). The *Chandra* (pink circle) X-ray error region is also shown, indicating that the VLA and *Chandra* localizations of the source are consistent.

using the 3-bit samplers at X-band (8–12 GHz), and were comprised of two basebands, each with 16 spectral windows of sixty-four 2 MHz channels, providing a total bandwidth of 2.048 GHz per base-band. We carried out flagging, calibration, and imaging within the Common Astronomy Software Application package (CASA, v5.1.1; McMullin et al. 2007), using standard procedures outlined in the CASA Guides¹⁰ for VLA data reduction (i.e., apriori flagging, re-quantizer gain corrections, setting the flux density scale, initial phase calibration, solving for antenna-based delays, bandpass calibration, gain calibration, scaling the amplitude gains, and final target flagging). When imaging we used a natural weighting scheme to maximize sensitivity and two Taylor terms ($n_{\text{terms}} = 2$) to account for the large fractional bandwidth. We used 3C 286 (J1331+305) as a flux calibrator and J1717-3948 as a phase calibrator (with a cycle time of 9 minutes on source, and 1 minute on the calibrator).

We significantly detect a radio source at a position consistent with the *Swift* X-ray position reported in Bozzo et al. (2017b) (see Figure 1). In the combined 4 GHz of bandwidth centered

¹⁰ <https://casaguides.nrao.edu>

on 10 GHz, we measure flux densities of $17.7 \pm 4.4 \mu\text{Jy}$ and $24.4 \pm 4.3 \mu\text{Jy}$ on October 23 and 27, respectively. To measure these flux densities we fit a point source in the image plane (with the `imfit` task). The fluxes were too low to obtain a meaningful constraint on the radio spectral index using images of the two individual basebands. The corresponding radio luminosities are shown in Table 1.

Additionally, we searched for intra-observation variability within both epochs of VLA data, on timescales as short as 30 minutes, which is the shortest timescale we can probe given the low source brightness. In both observations, the variance in the data points is consistent with the measurement uncertainties; we thus find no statistically significant evidence for flux variability on intra-observation timescales.

2.2. Swift X-Ray Observations of IGR J16597–3704

IGR J16597–3704 was observed with *Swift*/XRT twice following its detection with *INTEGRAL*. These observations occurred on 2017 October 22 in photon counting mode (PC; which produces two-dimensional images), and 2017 October 25 in windowed timing mode (WT; which collapses data to one dimension for fast readout). Observation times are displayed in Table 1.

We used HEASOFT v6.22 and FTOOLS¹¹ (Blackburn 1995) for all data reduction and analysis. All *Swift*/XRT observations were reprocessed via `xrtpipeline`, and `xselect` was used to manually extract source and background spectra. We used `xrtmkarf` to produce ancillary response files. Finally, we performed spectral analysis using XSPEC 12.9.1n (Arnaud 1996).

The PC mode observation was piled up. Therefore, we followed the recommended procedure for handling pile-up,¹² and extracted a source spectrum from an annulus, excluding the piled-up region (estimated to be ~ 10 arcsec), out to 80 arcsec. Following the recommended procedure for *Swift*/XRT data analysis, we used events from grades 0–12, and performed spectral analysis in the 0.3–10 keV band.

For the WT mode observation we used circular regions with a radius of ~ 47 arcsec (20 pixels) for both source and background. To minimize the effects of WT spectral residuals,¹³ we only extracted a spectrum from grade 0 events and performed spectral analysis in the 0.5–10 keV band, as these residuals become prominent around and below 0.5 keV.

We extracted the X-ray spectrum from each XRT observation separately to perform spectral fitting. Both of the XRT spectra are well fit with an absorbed power law (TBABS*PEGPWRLW in XSPEC), where we assume the photoelectric cross sections from Verner et al. (1996) and abundances from Wilms et al. (2000). We chose to use the TBABS ISM absorption model, as this model implements more recent estimates for the elemental abundance of the ISM, when compared with older models (e.g., PHABS or WABS; Bahramian et al. 2015; Foight et al. 2016). The best-fit spectral fitting parameters for both epochs are shown in Table 2, and the corresponding X-ray luminosities are shown in Table 1. We report 1σ confidence intervals on all fitted parameters. To calculate these 1σ confidence intervals, we first binned each

Table 2
Best-fit X-Ray Spectral Fitting Parameters for IGR J16597–3704

Epoch	N_H^a ($\times 10^{22} \text{ cm}^{-2}$)	Photon Index	$F_{1-10 \text{ keV}}^b$ ($\times 10^{-10} \text{ erg s}^{-1} \text{ cm}^{-2}$)
1	1.5 ± 0.2	1.5 ± 0.1	2.73 ± 0.11
2	1.1 ± 0.1	1.3 ± 0.1	2.80 ± 0.08

Notes.

^a Absorption column density.

^b Unabsorbed 1–10 keV flux.

spectrum to a minimum of 50 counts per bin using the `grppha` task, and utilized χ^2 statistics for spectral analysis. Following this analysis, the parameter uncertainties were estimated using the `error` task in XSPEC.¹⁴

2.3. Archival Optical and X-Ray Observations

We obtained archival X-ray and optical data of the field surrounding IGR J16597–3704 (see Figure 2), taken with the *Chandra* X-ray Observatory and the *Hubble Space Telescope* (*HST*). *Chandra* data were taken on 2008 January 26 (13:09:51 UTC start time, 9.4 ks exposure time, Obs ID: 8951) with the ACIS-S instrument. We reprocessed the data using CIAO v4.9 (Fruscione et al. 2006). *HST* images were obtained from the Hubble Legacy Archive (<http://hla.stsci.edu/>) in the F555W and F814W filters. These *HST* observations were taken with the WFC3/UVIS1 detector on 2009 August 02 (19:47:12/20:43:35 UTC start time, 1.1/0.3 ks exposure time, in the F555W/F814W filters). The absolute astrometry of the *HST* images was corrected by matching sources in the field to the GAIA catalog (Gaia Collaboration et al. 2016). We estimate that after matching to the GAIA catalog, the uncertainty in the absolute position registration of the *HST* images is $<0''.02$.

2.4. Additional Neutron Star Sources

We supplement¹⁵ these new radio/X-ray data on IGR J16597–3704 with our team’s recent radio/X-ray measurements of a number of other neutron star sources for further comparison: MAXI J0911-635 (Tudor et al. 2016), SAX J1748.9-2021 (Miller-Jones et al. 2010a; Tetarenko et al. 2017b), Swift J175233.9-290952 (Tetarenko et al. 2017c), and 4U 1543-624 (Ludlam et al. 2017). Additionally, we also include older detections of MAXI J0556-332 (Coriat et al. 2011b) and MXB 1730-335 (Rutledge et al. 1998) in this work. Table 3 displays a summary of the radio and X-ray luminosity measurements for these sources.

3. Results

3.1. Radio Source Position

Stacking both epochs of our VLA data in the *uv*-plane (see Figure 1) refines the radio position of IGR J16597–3704 to be

¹¹ <http://heasarc.gsfc.nasa.gov/ftools/>

¹² <http://www.swift.ac.uk/analysis/xrt/pileup.php>

¹³ For more details on these effects see the *Swift*/XRT calibration digest; http://www.swift.ac.uk/analysis/xrt/digest_cal.php#abs.

¹⁴ For details on how this task works see <https://heasarc.gsfc.nasa.gov/xanadu/xspec/manual/node80.html>.

¹⁵ The additional neutron star data reported in this section have only been reported in Astronomer’s Telegrams, and not previously published in refereed journals.

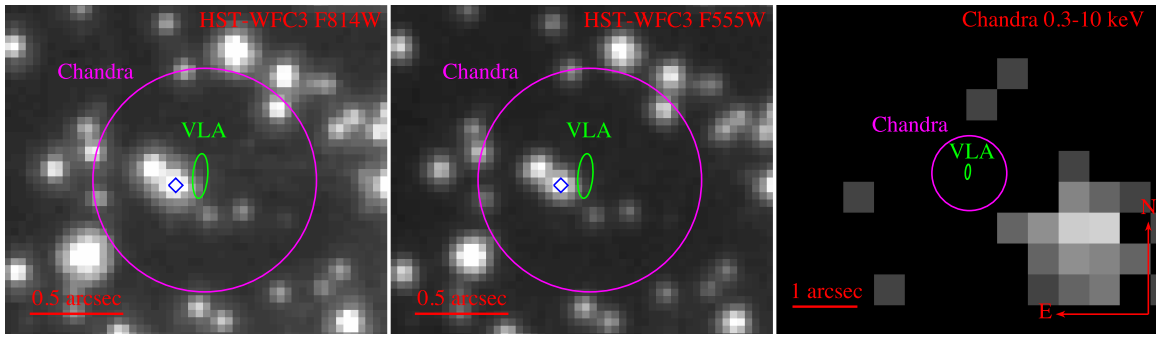


Figure 2. Archival *HST* and *Chandra* images of the field surrounding IGR J16597–3704. The left panel displays the *HST* F814W image, the middle panel displays the *HST* F555W image, and the right panel displays the *Chandra* (0.3–10 keV band) image. The *Chandra* (magenta circles), and VLA (green ellipses) error regions are indicated in all panels, and the blue diamonds indicate the possible counterpart discussed in Section 3.2. Note the different scales in the optical (left and middle) and X-ray (right) images. We do not detect an optical or quiescent X-ray counterpart to IGR J16597–3704 in these archival data.

Table 3
Radio and X-Ray Luminosities of Additional Neutron Star Sources

Source	$L_{5 \text{ GHz}}^{a,b}$ (erg s^{-1})	$L_{1-10 \text{ keV}}$ (erg s^{-1})	D^c (kpc)	References
MAXI J0911–635	$<4.5 \times 10^{28}$	2.5×10^{36}	10.4	(1)
SAX J1748.9–2021	$<4.5 \times 10^{27}$	2.1×10^{36}	8.5	(2)
	$<5.1 \times 10^{28}$	3.0×10^{37}		(3)
Swift J175233.9-290952	$<5.7 \times 10^{27}$	1.4×10^{34}	8.0	(4)
4U 1543–624	$<7.2 \times 10^{27}$	1.7×10^{37}	6.7	(5)
MAXI J0556–332	$<5.3 \times 10^{28}$	1.8×10^{37}	8.0	(6)
MXB 1730–335 ^d	$<2.0 \times 10^{28}$	6.1×10^{35}	8.6	(7)
	$<1.6 \times 10^{29}$	4.0×10^{37}		
	$<1.3 \times 10^{29}$	4.1×10^{37}		
	$<1.5 \times 10^{29}$	7.2×10^{37}		
	$<1.8 \times 10^{28}$	3.3×10^{36}		

Notes.

^a Upper limits are quoted at the 3σ level.

^b We calculate 5 GHz radio luminosities ($L_R = \nu L_\nu$) by assuming a flat spectral index to extrapolate to 5 GHz.

^c Distance value used to calculate luminosity.

^d Note that we use a model with $N_H = 1.7 \times 10^{22} \text{ cm}^{-2}$ (Marshall et al. 2001), and a photon index of 1.5, to convert from *RXTE* count rates to flux for this source.

References. (1) Tudor et al. (2016); (2) Tetarenko et al. (2017b); (3) Miller-Jones et al. (2010a); (4) Tetarenko et al. (2017c); (5) Ludlam et al. (2017); (6) Coriat et al. (2011b); (7) Rutledge et al. (1998).

the following (J2000):

$$\begin{aligned} \text{R.A.: } & 16^{\text{h}}59^{\text{m}}32^{\text{s}}.90230 \pm 0^{\text{s}}.00092 \pm 0^{\text{s}}.005 \\ \text{Decl.: } & -37^{\circ}07'14''.278 \pm 0''.088 \pm 0''.22, \end{aligned}$$

where the quoted errors represent the statistical error from fitting in the image plane and the nominal systematic uncertainties of 10% of the beam size, respectively. The elongated beam shape arises from the low declination of the source. This radio source position is consistent (within $0''.04$) with the best X-ray position of the source during outburst from *Chandra* (Chakrabarty et al. 2017).

3.2. Search for the Quiescent X-Ray and Optical Counterparts

We examined archival *Chandra* and *HST* observations in search of the quiescent X-ray and optical counterparts to IGR J16597–3704.

In the archival *Chandra* data, there is an X-ray source ~ 2.2 arcsec to the southwest of the VLA radio position (see the right panel of Figure 2). However, this *Chandra* source is unlikely to be the quiescent counterpart of IGR J16597–3704 given the typical *Chandra* absolute astrometric accuracy of 0.5 arcsec. To further confirm that the *Chandra* absolute astrometry is accurate (i.e., as good as 0.5 arcsec or better), we compare the positions of known X-ray sources in the cluster to their radio and optical counterparts. In particular, there is a radio continuum source ~ 2.5 arcmin from the center of the cluster that has a *Chandra* X-ray counterpart, and the positions match within 0.5 arcsec. Additionally, there are three X-ray sources in the outer regions of the cluster, where the optical source density is lower, that all clearly match bright stars present in the *Gaia* catalog. The individual offsets between the *Gaia* and *Chandra* positions vary from 0.6–1.0 arcsec, well within the uncertainties of the individual X-ray positions, and there is no evidence of a significant net astrometric shift. Together these arguments strongly suggest that the bright X-ray source in question is not associated with IGR J16597–3704, and that the quiescent counterpart of this transient is undetected in existing X-ray data.

We assert a non-detection in this *Chandra* observation and estimate a 95% upper limit on the count rate of $2.9 \times 10^{-4} \text{ cts s}^{-1}$. Assuming a distance of $D = 9.1 \text{ kpc}$ (Valenti et al. 2007), a hydrogen column density of $\sim 1.1 \times 10^{22} \text{ cm}^{-2}$, and a power-law spectrum (with a canonical photon index of 1.5), this translates to upper limits of $4.9 \times 10^{-15} \text{ erg s}^{-1} \text{ cm}^{-2}$ on the absorbed X-ray flux in the 0.5–10 keV band, and $L_X < 6.4 \times 10^{31} \text{ erg s}^{-1}$ for the luminosity, of the quiescent counterpart. Alternatively, assuming a neutron star atmosphere model (NSATMOS in XSPEC) with canonical values of $1.4M_\odot$ and a radius of 10 km, this translates to upper limits of $1.1 \times 10^{-15} \text{ erg s}^{-1} \text{ cm}^{-2}$ on the absorbed X-ray flux in the 0.5–10 keV band, and $L_X < 9.9 \times 10^{30} \text{ erg s}^{-1}$ for the luminosity. In this model, the upper limit on the absorbed flux corresponds to a neutron star temperature of $<75 \text{ eV}$. Neutron star temperatures have been measured in other systems to extend across a range of values, from $<50 \text{ eV}$ for the coolest neutron stars (e.g., EXO 1745–248, SAX J1808.4–3658, 1H 1905+000; Jonker et al. 2007; Heinke et al. 2009; Degenaar & Wijnands 2012), up to $\sim 150 \text{ eV}$ for the hottest neutron stars (e.g., XTE J1701–462; Wijnands et al. 2017). Our new temperature measurement indicates that the neutron star in IGR J16597–3704 is not an overly hot neutron star, but rather is

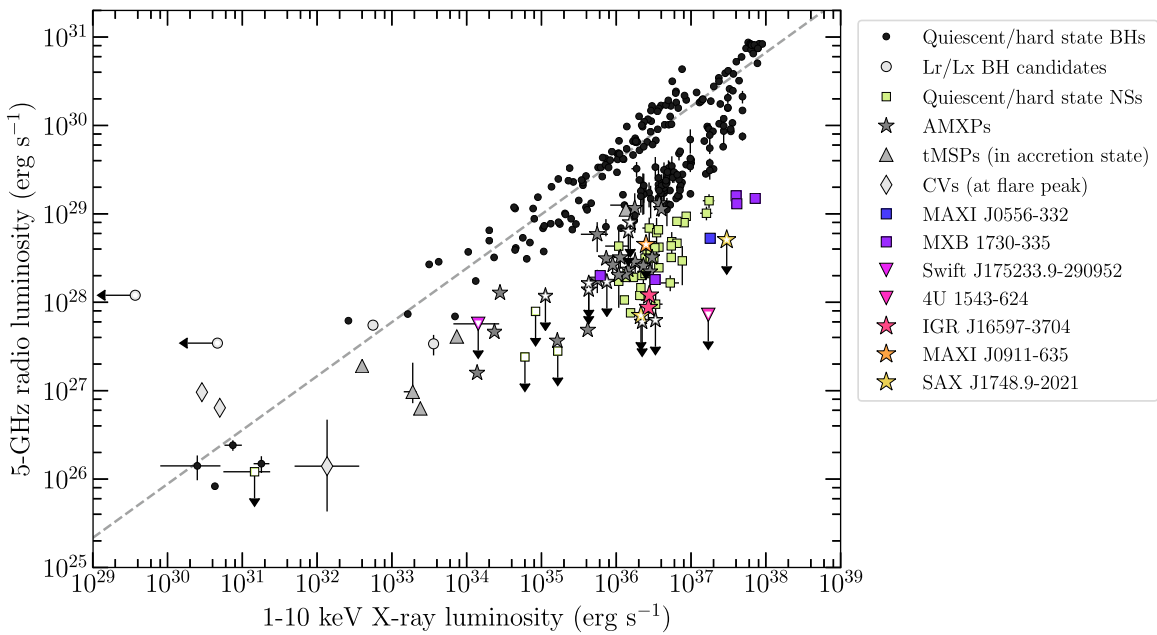


Figure 3. Radio–X-ray correlations for different types of accreting stellar-mass compact objects: black holes; different classes of neutron stars (non-pulsating NSXBs, AMXPs, and tMSPs); and out-bursting cataclysmic variables. This plot is adapted from Bahramian et al. (2017), with additional measurements from more recent publications, as well as those displayed in Table 3; Rutledge et al. (1998), Gallo et al. (2006), Miller-Jones et al. (2010a), Coriat et al. (2011b), Russell et al. (2015), Marsh et al. (2016), Tetarenko et al. (2016), Rushton et al. (2016), Tudor et al. (2016), Ribó et al. (2017), Plotkin et al. (2017), Tudor et al. (2017), Tetarenko et al. (2017b), Gusinskaia et al. (2017), Tetarenko et al. (2017c), Ludlam et al. (2017), Bogdanov et al. (2017), and Dincer et al. (2017). The best-fit relation for black holes ($\beta = 0.61$, gray dashed; Gallo et al. 2014) is also shown. Our measurements of IGR J16597–3704 and the measurements of other NSXBs reported in Table 3 are displayed with colored symbols (where non-pulsating NSXBs, AMXPs, and unclassified sources are indicated by the square, star, and inverted triangle shapes, respectively). IGR J16597–3704 (pink star shapes) is one of the more radio-quiet systems in the NSXB population.

consistent with an average or lower temperature neutron star, when compared with the current measured population.

In the *HST* data, there is no clear optical source within the VLA error circle (see Figure 2 left and middle). However, we identify a bright optical source $0''.13$ to the SE of our VLA radio position, which lies outside the 1σ VLA confidence interval. Optical photometry indicates this *HST* source was at $m_{F555W/F814W} \sim 22.4/20.3$ (AB magnitudes) on 2009 August 02, consistent with a typical giant star within the NGC 6256 cluster. Given that IGR J16597–3704 has been recently identified (Sanna et al. 2017) to be an ultra-compact system (which typically have compact white dwarf companions), this *HST* source is unlikely to be the optical counterpart. Therefore, the optical counterpart is probably too faint to be detected in the existing *HST* data. We estimate 3σ upper limits from the archival *HST* images of $m_{F555W/F814W} < 26.0/23.4$.

3.3. Radio–X-Ray Correlation

To explore the nature of IGR J16597–3704, we place our observations on the radio–X-ray plane, using the 5 GHz radio luminosity and the 1.0–10 keV X-ray luminosity (where that frequency and band are chosen to match measurements from the literature; see Figure 3 and Table 1).

The location of IGR J16597–3704 on the radio–X-ray plane lies at least an order of magnitude below most BHXBs, and instead is more consistent with neutron star systems (both non-pulsating NSXBs and AMXPs/tMSPs; see Figure 3). The recent detection of X-ray pulsations from this source with *NuSTAR* (Sanna et al. 2017), confirms that IGR J16597–3704 is a new AMXP source. All of the neutron star sources presented in this work display a significant range in radio luminosity. In particular, IGR J16597–3704, along with SAX

J1748.9-2021, Swift J175233.9-290952, and 4U 1543-624, display radio luminosities that are at the low end of the sampled NSXB population, while MAXI J0911-635, MAXI J0556-332, and MXB 1730-335 display radio luminosities at the mid-to-high end of the sampled NSXB population.

4. Discussion

In this paper, we have reported on the discovery of the radio counterpart to the new AMXP, IGR J16597–3704, located in the NGC 6256 globular cluster. We do not conclusively identify an optical or quiescent X-ray counterpart to IGR J16597–3704 in archival *HST* and *Chandra* data; our 3σ upper limits are $m_{F555W/F814W} < 26.0/23.4$ and $L_X < 6.1 \times 10^{31} \text{ erg s}^{-1}$.

Our recent radio observations indicate that IGR J16597–370 is one of the more radio faint systems in the NSXB population. For example, IGR J16597–3704 displays a similar radio luminosity to IGR J17511–3057 (AMXP; Tudor et al. 2017), SAX J1748.9–2021 (AMXP; Tetarenko et al. 2017b), and EXO 1745–248 (non-pulsating NSXB; Tetarenko et al. 2016). Examining our updated radio–X-ray plane figure (Figure 3), it is clear that both non-pulsating NSXBs and AMXPs can display a range of radio luminosities at a similar X-ray luminosity (where it is unclear whether the radio-brighter or radio-fainter systems form the dominant population). Here, we postulate on the mechanisms driving the radio luminosity in IGR J16597–3704 (and potentially other AMXPs) by exploring the relationships between radio luminosity and spectral state, spin, magnetic field, orbital period, accretion regime, and evolutionary state.

The jets from some NSXBs (like BHXBs) have been observed to be quenched by over an order of magnitude (or faded below current detection limits; e.g., Migliari et al. 2003; Gusinskaia et al. 2017) during softer accretion states. As such, we may

naively expect radio jets to be fainter in these states when compared to their harder accretion states. Since the X-ray spectral properties reported in Section 2.2 suggest that IGR J16597–3704 was in a canonical hard state during our observations, it is unlikely that jet quenching in the soft accretion state explains the low radio luminosity of IGR J16597–3704. By extension, many other radio quieter systems in the sampled population, such as EXO 1745–248 (Tetarenko et al. 2016), have also been observed firmly in the hard accretion state.

Sanna et al. (2017) have shown that IGR J16597–3704 displays a longer spin period (9.5 ms), when compared to the average values for AMXPs (Patruno & Watts 2012; Mukherjee et al. 2015; Patruno et al. 2017a, 2017b). The spin of a neutron star has long been suggested to potentially affect the radio luminosity of NSXBs (Migliari et al. 2011). Depending on how the magnetic field (anchored to the NS magnetic poles) interacts with the accretion disk, AMXP jets could be directly powered by the extraction of energy from the spin of the neutron star, or the jet may be driven by the rotation power of the accretion disk (Migliari et al. 2011, 2012). In both cases, we expect the neutron star spin period to correlate with jet power. For example, a longer spin period could be linked to a lower radio luminosity in AMXPs, analogous to the spin dependence of jet power for black holes ($L_{\text{jet}} \propto a^2$, where a is the black hole spin parameter) predicted by Blandford & Znajek 1977. Past studies (Migliari et al. 2011) have found hints of a possible positive correlation¹⁶ between spin frequency of the neutron star and jet power in AMXPs, and our measurements of IGR J16597–3704 are compatible with this scaling. Therefore, it seems plausible that spin period may play a role in governing the radio luminosity levels in IGR J16597–3704 (and potentially other radio-quiet AMXPs).

Similar to the spin period, IGR J16597–3704 may also display a higher magnetic field ($9.2 \times 10^8 < B < 5.2 \times 10^{10}$ G) when compared to the average values for AMXPs. The role of a high magnetic field in jet production is still an open question. Past works have suggested that high magnetic fields ($\gtrsim 10^{11}$ G; Fender & Hendry 2000; Migliari et al. 2012) may inhibit jet formation, but the recent work by van den Eijnden et al. (2018a, 2018b; described below) provides a counterpoint, thus we explore both possibilities here. Using the condition that the gas pressure must dominate over the magnetic pressure, Massi and Kaufman Bernadó (2008) derive a condition for jet formation based on the magnetic field strength (B_*) and accretion rate (\dot{M}), such that,

$$\frac{R_A}{R_*} = 0.87 \left(\frac{B_*}{10^8 \text{ G}} \right)^{4/7} \left(\frac{\dot{M}}{10^{-8} M_\odot \text{ yr}^{-1}} \right)^{-2/7}, \quad (1)$$

where R_A is the Alfvén radius, and $\frac{R_A}{R_*} \approx 1$ indicates the portion of the parameter space where jet formation is likely to not be suppressed by the neutron star magnetic field. Substituting in estimates of $9.2 \times 10^8 < B_* < 5.2 \times 10^{10}$ G (Sanna et al. 2017) and $\dot{M} = 5 \times 10^{-12} M_\odot \text{ yr}^{-1}$ (estimated from the \dot{M}/P_{orb} relationship reported in van Haften et al. 2012¹⁷) for IGR J16597–3704, indicates that IGR J16597

–3704 may be in a regime ($\frac{R_A}{R_*} > 1$) where the magnetic field could potentially be inhibiting jet formation (and in turn lead to the lower radio luminosity observed).

Contrary to this hypothesis, radio emission (consistent with a synchrotron jet) has been recently detected in the high magnetic field neutron star systems GX 1 + 4 (van den Eijnden et al. 2018a) and Her X-1 (van den Eijnden et al. 2018b). Moreover, another AMXP, IGR J17511–43057, displays a magnetic field strength similar to the average AMXP population, but lower than average radio luminosity (Tudor et al. 2017). Furthermore, if high magnetic fields are linked to lower radio luminosities in neutron stars, we may expect that the AMXP population in general would display lower radio luminosities compared to the population of non-pulsating NSXBs (which presumably display lower magnetic fields than pulsating systems). This is clearly not the case, as, for example, the non-pulsating NSXB EXO 1745–248 displays a radio luminosity similar to that of IGR J16597–3704 (also see Figure 3). Therefore, there does not appear to be a clear relationship between the magnetic field strength of the neutron star and radio luminosity in the current sampled population, suggesting that the high magnetic field in IGR J16597–3704 does not strongly influence the radio luminosities we observe.

However, if different jet production mechanisms are at work in different classes of neutron star systems, we may expect a much more complicated (beyond a simple scaling) relationship between the magnetic field strength of the neutron star and the radio luminosity. For instance, the jet production mechanism in neutron star systems could be highly dependent on how dynamically important the magnetic field of the neutron star is in each system (i.e., how significant a role the stellar magnetic fields play in the accretion process). In this case, jets launched from non-pulsating NSXBs, with dynamically unimportant magnetic fields, may be powered by the accretion disk, similar to BHXBs, while the dynamically important magnetic fields in tMSPs/AMXPs could disrupt this physical connection between the jet and the disk. Therefore, in some systems we may not be observing an accretion-powered jet, but rather another mechanism, such as the propeller effect¹⁸ (Romanova et al. 2009; Parfrey et al. 2017), which may be powering the jet (e.g., the propeller effect is thought to be the origin of the anti-correlation between radio and X-ray luminosity observed in PSR J1023+0038; Bogdanov et al. 2017).

Because IGR J16597–3704 is an ultra-compact binary (with an orbital period <80 minutes), we opt to briefly investigate a possible link between radio luminosity and orbital period by compiling a list of all the ultra-compact neutron star binaries with radio frequency measurements (see Table 4 and Figure 4). We find that in these ultra-compact binaries, the orbital period does not appear to be correlated with the position of the system in the radio–X-ray plane. Furthermore, we also find no evidence of a direct correlation between orbital period and radio luminosity (Spearman rank correlation coefficient of -0.22 , and p -value of 0.46). This suggests that orbital period may not play a key role in governing the radio luminosity in IGR J16597–3704 or other systems.

Lastly, the radio luminosity in AMXPs may be closely tied to the evolutionary state or the accretion regime (i.e., X-ray spectral state and mass accretion rate, as suggested by Migliari et al. 2011) of the system. In IGR J16597–3704, Sanna et al.

¹⁶ However, we note that the jet power was not measured directly in this work, with the normalization of the sources on the radio X-ray plane (assuming a disk-jet coupling index of 1.4) being used as a proxy for jet power. Thus, this correlation may break down for different disk-jet coupling indices.

¹⁷ While Sanna et al. (2017) report an $\dot{M} = 5.5 \times 10^{-10} M_\odot \text{ yr}^{-1}$, this estimate only represents the peak \dot{M} in the outburst.

¹⁸ In the case of the propeller effect, the radio emission may originate in a broader outflow, as opposed to a well-collimated jet.

Table 4
Properties of Ultra-compact Neutron Star Binaries

Source	$L_{5\text{ GHz}}^{\text{a,b}}$ (erg s^{-1})	$L_{1-10\text{ keV}}^{\text{a}}$ (erg s^{-1})	$D^{\text{c,d}}$ (kpc)	$P_{\text{orb}}^{\text{d}}$ (min)	References
4U1728-34	6.83×10^{28}	5.2×10^{36}	5.2	$10.8^{?g}$	(1)
4U 1820-303	8.78×10^{28}	9.7×10^{36}	7.9	11	(1)
4U 0513-40	$<5.50 \times 10^{28}$	2.9×10^{36e}	12.1	17	(2)
2S0918-549	$<5.21 \times 10^{28}$	9.5×10^{35e}	5.4	17.4	(3)
4U 1543-624	$<7.20 \times 10^{27}$	1.7×10^{37}	6.7	18.2	(4)
4U 1850-087	4.60×10^{28}	1.2×10^{36e}	6.9	20.6	(5)
M15 X-2	3.67×10^{28}	2.3×10^{37}	10.4	22.6	(6)
4U 1916-053	$<1.80 \times 10^{29}$	2.7×10^{36e}	9.3	50	(7)
4U 0614+091	1.72×10^{28}	3.2×10^{36}	3.2	$51^{?g}$	(8)
XTE J1751-305	$<1.14 \times 10^{28}$	$<2.3 \times 10^{32f}$	8.0	42	(9)
XTE J0929-314	1.37×10^{29}	4.7×10^{36}	8.0	43.6	(10)

Notes.

^a Upper limits are quoted at the 3σ level.

^b We calculate 5 GHz radio luminosities ($L_R = \nu L_\nu$) by assuming a flat spectral index to extrapolate to 5 GHz.

^c Distance value used to calculate luminosity.

^d All distance and orbital period measurements are taken from Cartwright et al. (2013).

^e These systems did not have X-ray measurements reported with their radio measurements; we place limits on the X-ray luminosity by using the luminosity functions reported in Cartwright et al. (2013).

^f XTE J1751-305 did not have an X-ray measurement reported with its radio measurement; we use the upper limit on the quiescent X-ray luminosity reported in Wijnands et al. (2005).

^g Cartwright et al. (2013) classified these estimates of orbital period as more uncertain, as they are supported by only weak evidence.

References. (1) Díaz Trigo et al. (2017); (2) Machin et al. (1990); (3) Zwarthoed et al. (1993); (4) Ludlam et al. (2017); (5) Lehto et al. (1990); (6) Sivakoff et al. (2011); (7) Grindlay & Seaquist (1986); (8) Migliari et al. (2010); (9) Iacolina et al. (2010); (10) Rupen et al. (2002).

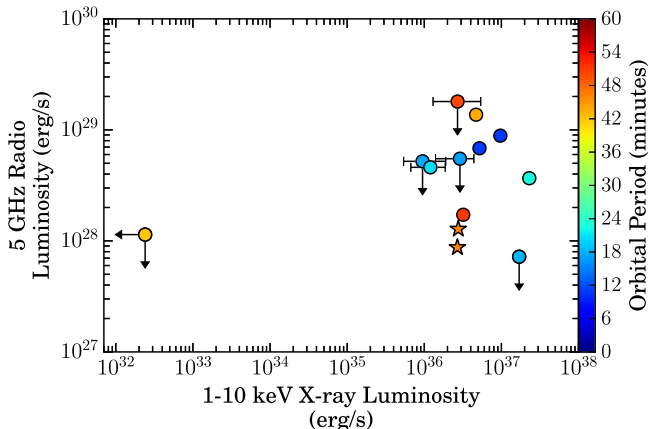


Figure 4. Radio–X-ray correlation for ultra-compact neutron star binaries. The data points are color-coded by orbital period. Our IGR J16597–3704 measurements are indicated by the star symbols. The data points with horizontal error bars represent those systems for which the X-ray luminosity measurements were estimated from luminosity functions or quiescent X-ray limits (see Table 4 for details). We observe no clear correlation between the position of these sources on the radio–X-ray plane and orbital period.

(2017) estimate that very little mass has been accreted so far in the system, and suggest that this indicates it is in an early stage of its evolution (i.e., it is a partially recycled pulsar). However, the likelihood of catching this system in such a short-lived early evolutionary state is quite low. Since IGR J16597–3704 is an ultra-compact binary (with a low donor star mass; Sanna et al. 2017), it is much more consistent with a system in the later stages of its evolution. This uncertainty makes it difficult to postulate whether the evolutionary state of IGR J16597–3704 (and other AMXPs) influences their observed radio luminosities, without further study.

A larger sample of radio luminosity constraints from AMXPs is needed to definitively determine whether the spectral state,

spin period, magnetic field strength, orbital period, or accretion regime/evolutionary state are linked to jet behavior.

Overall, these results highlight the need for more radio and X-ray measurements of all classes of NSXBs to place improved constraints on the mechanisms that govern radio luminosity, jet production, and jet evolution in NSXBs. The low X-ray luminosity regime ($L_X < 10^{36}$ erg s $^{-1}$) is particularly vital, as this regime remains undersampled for the different classes of NSXBs. Finally, despite the lack of a clear correlation for neutron star systems, IGR J16597–3704 is a clear example that the radio–X-ray plane can still be a reliable diagnostic to identify the nature of the accretor in these binary systems.


We thank the National Radio Astronomy Observatory and *Swift* staff for rapidly scheduling the observations reported in this paper. The authors thank Lennart van Haften for a helpful discussion on binary evolution models and Vlad Tudor for his help compiling radio and X-ray measurements of additional neutron star systems for this work. A.J.T. is supported by a Natural Sciences and Engineering Research Council of Canada (NSERC) Post-Graduate Doctoral Scholarship (PGSD2-490318-2016). A.J.T., G.R.S., C.O.H., and A.W.S. are supported by NSERC Discovery Grants. J.C.A.M.J. is the recipient of an Australian Research Council Future Fellowship (FT140101082). R.M.P. acknowledges support from Curtin University through the Peter Curran Memorial Fellowship. N.D. is supported by a Vidi grant from the Netherlands Organisation for Scientific Research (NWO). T.D.R. acknowledges support from the NWO Veni Fellowship. J.S. acknowledges support from the Packard Foundation. J.A.K. acknowledges support from the NASA contract NAS5-00136. The National Radio Astronomy Observatory is a facility of the National Science Foundation operated under cooperative agreement by Associated Universities, Inc. This work has made use of data from the European Space Agency (ESA) mission *Gaia* (<https://www.cosmos.esa.int/gaia>), processed by the *Gaia* Data

Processing and Analysis Consortium (DPAC, <https://www.cosmos.esa.int/web/gaia/dpac/consortium>). Funding for DPAC has been provided by national institutions, in particular the institutions participating in the *Gaia* Multilateral Agreement. This research has made use of the following data and software packages: Swift XRT Data Analysis Software (XRTDAS) developed under the responsibility of the ASI Science Data Center (ASDC), Italy. We acknowledge extensive use of ADS and arXiv.

Facilities: VLA, *Swift* (XRT), *HST* (WFC3/UVIS1), *Chandra* (ACIS-S).

Software: CASA, (v5.1.1; McMullin et al. 2007), HEASOFT (v6.2.2; Blackburn 1995), FTOOLS (Blackburn 1995), XSPEC (12.9.1n; Arnaud 1996), CIAO (v4.9; Fruscione et al. 2006).

ORCID iDs

A. J. Tetarenko  <https://orcid.org/0000-0003-3906-4354>
 A. Bahramian  <https://orcid.org/0000-0003-2506-6041>
 C. O. Heinke  <https://orcid.org/0000-0003-3944-6109>
 J. C. A. Miller-Jones  <https://orcid.org/0000-0003-3124-2814>
 J. Strader  <https://orcid.org/0000-0002-1468-9668>
 L. Chomiuk  <https://orcid.org/0000-0002-8400-3705>
 G. R. Sivakoff  <https://orcid.org/0000-0001-6682-916X>
 D. Altamirano  <https://orcid.org/0000-0002-3422-0074>
 A. T. Deller  <https://orcid.org/0000-0001-9434-3837>
 J. A. Kennea  <https://orcid.org/0000-0002-6745-4790>
 K. L. Li  <https://orcid.org/0000-0002-0439-7047>
 R. M. Plotkin  <https://orcid.org/0000-0002-7092-0326>
 T. D. Russell  <https://orcid.org/0000-0002-7930-2276>
 A. W. Shaw  <https://orcid.org/0000-0002-8808-520X>

References

- Archibald, A. M., Stairs, I. H., Ransom, S. M., et al. 2009, *Sci*, **324**, 1411
 Arnaud, K. 1996, in ASP Conf. Ser. 101, *Astronomical Data Analysis Software and Systems V*, ed. G. H. Jacoby & J. Barnes (San Francisco, CA: ASP), 17
 Bahramian, A., Heinke, C., Degenaar, N., et al. 2015, *MNRAS*, **452**, 3475
 Bahramian, A., Heinke, C. O., Tudor, V., et al. 2017, *MNRAS*, **467**, 2199
 Bassa, C. G., Patruno, A., Hessels, J. W. T., et al. 2014, *MNRAS*, **441**, 1825
 Blackburn, J. 1995, in ASP Conf. Ser. 77, *Astronomical Data Analysis Software and Systems IV*, ed. R. A. H. J. J. E. Shaw & H. E. Payne (San Francisco, CA: ASP), 367
 Blandford, R., & Znajek, R. 1977, *MNRAS*, **179**, 433
 Bogdanov, S., Deller, A. T., Miller-Jones, J. C. A., et al. 2017, arXiv:1709.08574
 Bozzo, E., Grinberg, V., Wilms, J., et al. 2017a, *ATel*, **10880**, 1
 Bozzo, E., Grinberg, V., Wilms, J., et al. 2017b, *ATel*, **10881**, 1
 Burrows, D. N., Hill, J. E., Nousek, J. A., et al. 2005, *SSRv*, **120**, 165
 Cartwright, T. F., Engel, M. C., Heinke, C. O., et al. 2013, *ApJ*, **768**, 183
 Chakrabarty, D., Jonker, P., & Markwardt, C. 2017, *ATel*, **10898**, 1
 Coppejans, D., Körding, E., Miller-Jones, J., et al. 2015, *MNRAS*, **451**, 3801
 Corbel, S., Coriat, M., Brocksopp, C., et al. 2013, *MNRAS*, **428**, 2500
 Coriat, M., Corbel, S., Prat, L., et al. 2011a, *MNRAS*, **414**, 677
 Coriat, M., Tzioumis, T., Corbel, S., et al. 2011b, *ATel*, **3119**, 1
 Degenaar, N., & Wijnands, R. 2012, *MNRAS*, **422**, 581
 Deller, A. T., Moldon, J., Miller-Jones, J. C. A., et al. 2015, *ApJ*, **809**, 13
 Díaz Trigo, M., Migliari, S., Miller-Jones, J. C. A., et al. 2017, *A&A*, **600**, A8
 Dincer, T., Bailyn, C. D., Miller-Jones, J. C. A., Buxton, M., & MacDonald, R. K. D. 2018, *ApJ*, **852**, 4
 Fender, R. 2006, in *Compact Stellar X-ray Sources*, ed. W. H. G. Lewin & M. van der Klis (Vol. 39; Cambridge: Cambridge Univ. Press)
 Fender, R. P., & Hendry, M. A. 2000, *MNRAS*, **317**, 1
 Foight, D. R., Güver, T., Özel, F., & Slane, P. O. 2016, *ApJ*, **826**, 66
 Fruscione, A., McDowell, J. C., Allen, G. E., et al. 2006, *Proc. SPIE*, **6270**, 62701V
 Gaia Collaboration, Prusti, T., de Bruijne, J. H. J., et al. 2016, *A&A*, **595**, A1
 Gallo, E., Fender, R. P., Miller-Jones, J. C. A., et al. 2006, *MNRAS*, **370**, 1351
 Gallo, E., Fender, R. P., & Pooley, G. 2003, *MNRAS*, **344**, 60
 Gallo, E., Miller-Jones, J. C. A., Russell, D., et al. 2014, *MNRAS*, **445**, 290
 Grindlay, J. E., & Seaquist, E. R. 1986, *ApJ*, **310**, 172
 Gusinskaia, N. V., Deller, A. T., Hessels, J. W. T., et al. 2017, *MNRAS*, **470**, 1871
 Heinke, C. O., Jonker, P. G., Wijnands, R., Deloye, C. J., & Taam, R. E. 2009, *ApJ*, **691**, 1035
 Iacolina, M. N., Burgay, M., Burderi, L., Possenti, A., & di Salvo, T. 2010, *A&A*, **519**, A13
 Jonker, P. G., Steeghs, D., Chakrabarty, D., & Juett, A. M. 2007, *ApJL*, **665**, L147
 Körding, E., Rupen, M., Knigge, C., et al. 2008, *Sci*, **320**, 1318
 Lehto, H. J., Machin, G., McHardy, I. M., & Callanan, P. 1990, *Natur*, **347**, 49
 Ludlam, R., Miller, J. M., Miller-Jones, J., & Reynolds, M. 2017, *ATel*, **10690**, 1
 Machin, G., Lehto, H. J., McHardy, I. M., Callanan, P. J., & Charles, P. A. 1990, *MNRAS*, **246**, 237
 Marsh, T. R., Gänsicke, B. T., Hümmerich, S., et al. 2016, *Natur*, **537**, 374
 Marshall, H. L., Rutledge, R., Fox, D. W., et al. 2001, *AJ*, **122**, 21
 Massi, M., & Kaufman Bernadó, M. 2008, *A&A*, **477**, 1
 McMullin, J., Waters, B., Schiebel, D., Young, W., & Golap, K. 2007, in ASP Conf. Ser. 376, *Astronomical Data Analysis Software and Systems XVI*, ed. R. Shaw, F. Hill, & D. Bell (San Francisco, CA: ASP), 127
 Migliari, S., & Fender, R. 2006, *MNRAS*, **366**, 79
 Migliari, S., Fender, R. P., Rupen, M., et al. 2003, *MNRAS*, **342**, L67
 Migliari, S., Ghisellini, G., Miller-Jones, J., & Russell, D. 2012, *International Journal of Modern Physics Conference Series*, **8**, 108
 Migliari, S., Miller-Jones, J. C. A., & Russell, D. M. 2011, *MNRAS*, **415**, 2407
 Migliari, S., Tomsick, J. A., Miller-Jones, J. C. A., et al. 2010, *ApJ*, **710**, 117
 Miller-Jones, J. C. A., Heinke, C. O., Sivakoff, G. R., et al. 2010a, *ATel*, **2377**, 1
 Miller-Jones, J. C. A., Sivakoff, G., Altamirano, D., et al. 2010b, *MNRAS*, **716**, L109
 Mukherjee, D., Bult, P., van der Klis, M., & Bhattacharya, D. 2015, *MNRAS*, **452**, 3994
 Papitto, A., Ferrigno, C., Bozzo, E., et al. 2013, *Natur*, **501**, 517
 Parfrey, K., Spitkovsky, A., & Beloborodov, A. M. 2017, *MNRAS*, **469**, 3656
 Patruno, A., Archibald, A. M., Hessels, J. W. T., et al. 2014, *ApJL*, **781**, L3
 Patruno, A., Haskell, B., & Andersson, N. 2017a, arXiv:1705.07669
 Patruno, A., & Watts, A. L. 2012, arXiv:1206.2727
 Patruno, A., Wette, K., & Messenger, C. 2017b, arXiv:1709.10408
 Plotkin, R. M., Bright, J., Miller-Jones, J. C. A., et al. 2017, *ApJ*, **848**, 92
 Ribó, M., Munar-Adrover, P., Paredes, J. M., et al. 2017, *ApJL*, **835**, L33
 Romanova, M. M., Ustyugova, G. V., Koldoba, A. V., & Lovelace, R. V. E. 2009, *MNRAS*, **399**, 1802
 Rupen, M. P., Dhawan, V., & Mioduszewski, A. J. 2002, *IAUC*, **7893**, 1
 Rushton, A. P., Shaw, A., Fender, R. P., et al. 2016, *MNRAS*, **463**, 628
 Russell, T. D., Miller-Jones, J. C. A., Curran, P. A., et al. 2015, *MNRAS*, **450**, 1745
 Russell, T. D., Miller-Jones, J. C. A., Sivakoff, G. R., et al. 2016, *MNRAS*, **460**, 3720
 Rutledge, R., Moore, C., Fox, D., Lewin, W., & van Paradijs, J. 1998, *ATel*, **8**, 1
 Sanna, A., Bahramian, A., Bozzo, E., et al. 2017, arXiv:1711.03092
 Sivakoff, G. R., Heinke, C. O., Miller-Jones, J. C. A., et al. 2011, *ATel*, **3393**, 1
 Tetarenko, A. J., Bahramian, A., Sivakoff, G. R., et al. 2016, *MNRAS*, **460**, 345
 Tetarenko, A. J., Bahramian, A., Sivakoff, G. R., et al. 2017a, *ATel*, **10894**, 1
 Tetarenko, A. J., Bahramian, A., Sivakoff, G. R., et al. 2017b, *ATel*, **10843**, 1
 Tetarenko, A. J., Sivakoff, G. R., Heinke, C. O., et al. 2017c, *ATel*, **10422**, 1
 Tudor, V., Bahramian, A., Sivakoff, G., et al. 2016, *ATel*, **8914**, 1
 Tudor, V., Miller-Jones, J. C. A., Patruno, A., et al. 2017, *MNRAS*, **470**, 324
 Tudose, V., Fender, R. P., Linares, M., Maitra, D., & van der Klis, M. 2009, *MNRAS*, **400**, 2111
 Valenti, E., Ferraro, F. R., & Origlia, L. 2007, *AJ*, **133**, 1287
 van den Eijnden, J., Degenaar, N., Russell, T. D., et al. 2018a, *MNRAS*, **474**, L91
 van den Eijnden, J., Degenaar, N., Russell, T. D., et al. 2018b, *MNRAS*, **473**, L141
 van Haften, L. M., Voss, R., & Nelemans, G. 2012, *A&A*, **543**, A121
 Verner, D. A., Ferland, G. J., Korista, K. T., & Yakovlev, D. G. 1996, *ApJ*, **465**, 487
 Wijnands, R., Degenaar, N., & Page, D. 2017, *JApA*, **38**, 49
 Wijnands, R., Homan, J., Heinke, C. O., Miller, J. M., & Lewin, W. H. G. 2005, *ApJ*, **619**, 492
 Wilms, J., Allen, A., & McCray, R. 2000, *ApJ*, **542**, 914
 Zwarthoed, G. A. A., Stewart, R., Penninx, W., et al. 1993, *A&A*, **267**, 101